



# Low Temperature Plasma Technology Laboratory

---

## **The low-field density peak in helicon discharges**

Francis F. Chen

*Electrical Engineering Department*

LTP-211

November, 2002



Electrical Engineering Department  
Los Angeles, CA 90095-1594

# The low-field density peak in helicon discharges

Francis F. Chen\*

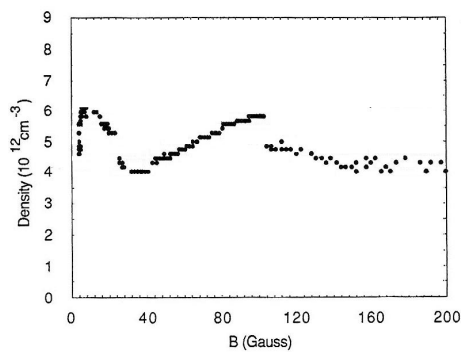
*Electrical Engineering Department, University of California, Los Angeles; Los Angeles, California 90095-1597*

## ABSTRACT

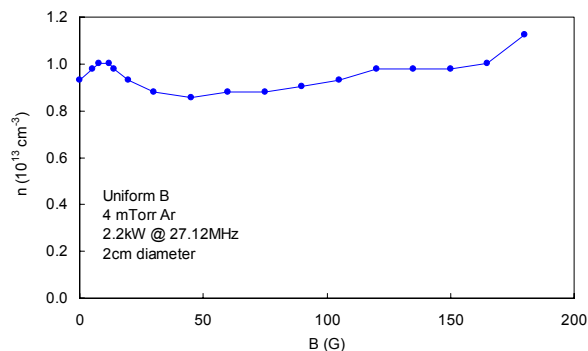
Although the density  $n$  in helicon discharges increases monotonically with magnetic field  $B$  for  $B$  larger than a few hundred gauss, as expected from theory, a pronounced density peak is often observed at  $B \sim 50\text{G}$  or below. A peak in antenna loading is indeed found in computations using a fluid code as long as reflections from an endplate are taken into account. Various tests show that this peak is caused by constructive interference from the reflected wave. This effect can be used in the design of compact helicon plasma injectors. In addition, it can be the cause of density enhancements previously observed using cusped magnetic fields or aperture limiters.

## I. BACKGROUND

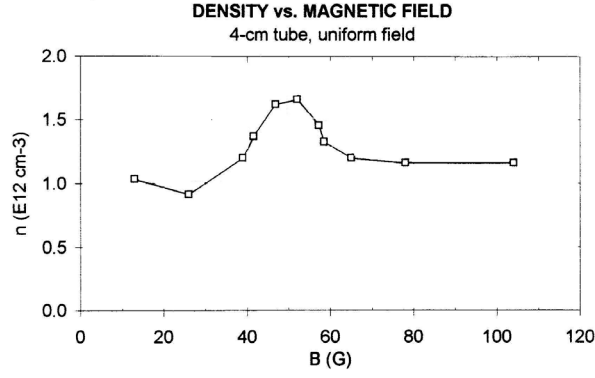
Helicon discharges have drawn interest because they can convert radiofrequency (rf) energy into plasma density more efficiently than other rf plasma sources. In general,  $n$  increases almost linearly with dc magnetic field  $B$ , but this dependence is violated at low  $B$ , where  $n(B)$  has a local peak for  $B$  around 10 – 50G and  $n$  of order  $10^{12}\text{ cm}^{-3}$ . This low- $B$  peak was first detected in our earliest experiments on helicons (Fig. 1) and has subsequently been seen in almost all helicon discharges in this range of  $n$  and  $B$ . This effect has also been seen in the downstream plasma created by a 7-tube array of helicon sources<sup>1</sup> (Fig. 2). Heretofore unexplained, this feature has a practical application in rf sources for fabrication of semiconductor circuits, since densities much exceeding  $10^{12}\text{ cm}^{-3}$  are not useful for this purpose, and the low value of  $B$  would make helicon reactors quite economical. The purpose of this paper is to show that the low- $B$  peak is caused by reflection from endplates and can be designed into helicon sources used to inject plasma into a processing chamber. Fig. 3 is a schematic of the type of plasma injector we envision, with an insulating or conducting back plate close to the antenna.



(a)

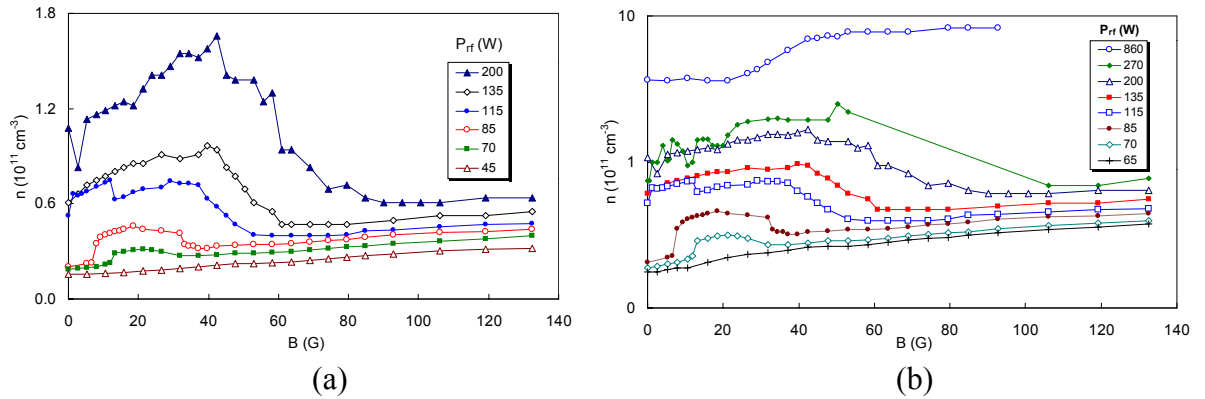


(b)



(c)

Fig. 1. Low- $B$  density peaks observed in a 2-cm diam helicon discharges in 1989 (a) and 1991 (b), and in a 4-cm discharge in 1992 (c).



(a)

(b)

Fig. 2. The low- $B$  peak observed in a 7-tube array of helicon sources at (a) low and (b) high  $P_{rf}$  for  $m = 0$  antennas at 8 mTorr of Ar and 13.56MHz (Ref. 1). The peak is not seen at higher  $P_{rf}$  (higher density).

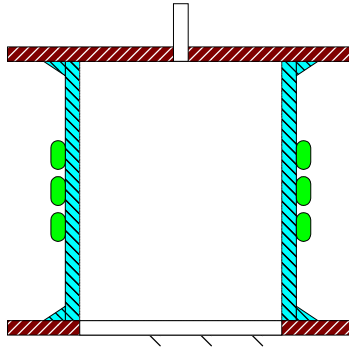


Fig. 3. A generic helicon injector with a generic antenna.

## II. COMPUTATIONS

A low- $B$  peak in plasma loading of an rf antenna is predictable by helicon codes as long as wave reflection from endplates is included. The code used here is the HELIC code of D. Arnush<sup>2</sup>, which is similar to many other collisional codes<sup>3-8</sup> used for helicon waves in that the plasma is represented by a cold-plasma dielectric tensor. The 2D HELIC code treats radial density profiles and coupling to the most common antennas, but the dc B-field must be uniform. In the latest version, the antenna can be located at an arbitrary position between

endplates, which can be conducting or insulating. The results obtained here should be reproducible by any other code with these simple features.

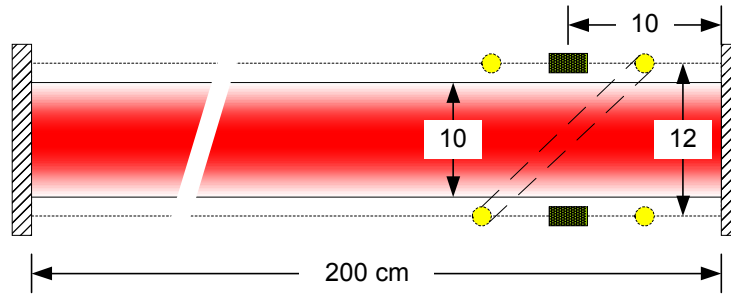


Fig. 4. Starting geometry used in the computations.

The starting geometry for the computations is shown in Fig. 4, and variations from this configuration will be studied. The plasma has a radius  $a = 5$  cm, and the antenna is a thin shell of radius 6 cm. The system is bounded by a conducting shell at a large radius of, say, 15 cm. The antenna is a single  $m = 0$  loop located at  $d = 10$  cm from the nearer endplate, which is an insulator. The other end is far away (200 cm) to simulate injection into an unbounded volume. When the  $m = 0$  antenna is replaced by an  $m = 1$  antenna of finite length,  $d$  is the distance from the midplane of the antenna to the endplate. The standard density profile is flat, with a roll-off at the edges, as is often found in experiment. This profile is shown by the heavy solid line in Fig. 5, as compared with parabolic and uniform profiles. Unless otherwise specified, standard conditions are  $n(0) = 10^{12}$  cm $^{-3}$  and  $B = 100$  G.

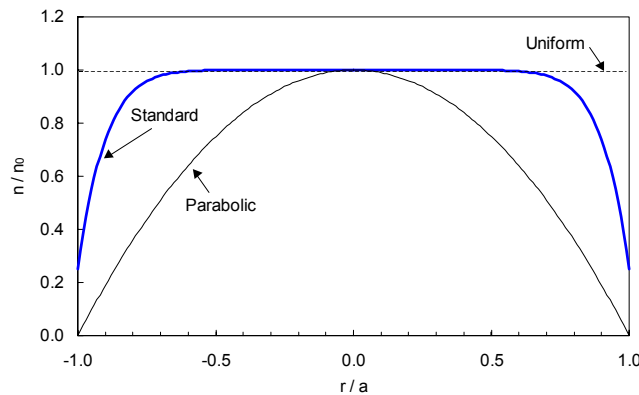


Fig. 5. Radial density profiles assumed in the computations. The heavy curve is the standard one used in most cases.

Figure 6 shows the spectrum of energy deposition vs. axial wavenumber  $k$  in the standard configuration with  $n = 10^{12}$  cm $^{-3}$  on axis and  $B = 50$  G.  $S(k)$  is the plasma response at each  $k$ , and  $P(k)$  is the net absorption including the antenna spectrum. The two peaks correspond to the first two radial modes of  $m = 0$  helicon waves. Figure 7 is the radial distribution of power deposition for the same conditions. A large peak in  $P(r)$  near the periphery due to the Trivelpiece-Gould (TG) mode<sup>2</sup> is seen, as is normal. This peak would be even larger when weighted by  $r$  to account for the solid angle. Figure 8 is the power deposition vs.  $z$ , with the insulating endplate at the left. For  $m = 0$  it is seen that  $P(z)$  peaks under the antenna and decays downstream with a scalelength of about 20 cm. The peak would be downstream from the antenna with an  $m = +1$  helical antenna, which launches waves in a preferred direction. The fields to the left of the antenna are enhanced by waves reflected from the endplate.

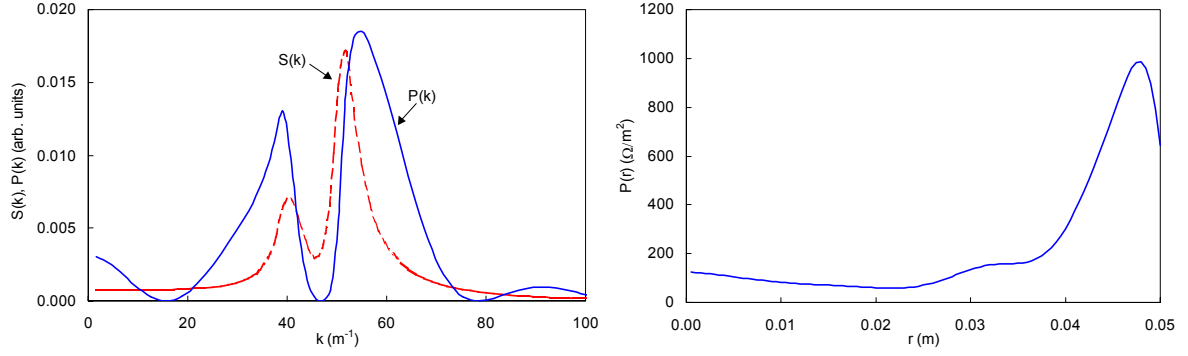


Fig. 6. The  $k$ -spectra of waves excited in the standard configuration.  $S(k)$  is the plasma response, and  $P(k)$  is the convolution of  $S(k)$  with the antenna spectrum.

Fig. 7. Energy deposition per unit area vs. radius (standard configuration).

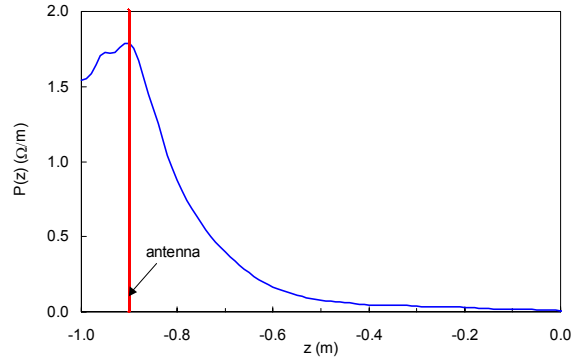


Fig. 8. Energy deposition vs.  $z$  (standard configuration). The line is the position of the single loop antenna.

### III. Results

The low- $B$  peak is clearly seen in computations of the plasma resistance  $R$ , in ohms, vs.  $B$  at various densities in the standard configuration (Fig. 9). Each point on these curves is computed as follows. For given  $k$ , a fourth-order differential equation in  $r$  is solved for the wave fields at that  $k$ , and integration over the  $k$ -spectrum gives the total wave field. Integration of  $\mathbf{J} \cdot \mathbf{E}$  over the plasma volume then gives the plasma loading. As a check,  $\mathbf{J} \cdot \mathbf{E}$  in the antenna is also calculated; it agrees to within  $<1\%$ . A clear peak in  $R$  is seen for  $2 \times 10^{11} < n < 2 \times 10^{12} \text{ cm}^{-3}$ . At higher densities, the peak moves to higher fields and becomes indistinct. This behavior is also observed in the experimental data of Fig. 2(b). In the density range where the peak is distinct, it occurs at a B-field increasing linearly with  $n$  (Fig. 10).

The curves of Fig. 9, however, are not those observed in experiment because they give the plasma resistance, not the density. The latter can be predicted only by codes that include ionization, diffusion, and circuit losses. As the loading changes,  $n$  would change at fixed power  $P_{\text{rf}}$  and  $B$ , and the plasma would jump to a curve of different  $n$ . An alternative representation is shown in Fig. 11, where  $R$  is plotted against  $n$  for fixed  $B$ . Consider, for instance, the curve at 50 G, where the peak in  $R$  is at  $n_{\text{max}}$ , say. If  $n > n_{\text{max}}$ , the energy deposition falls, and  $n$  will fall back towards  $n_{\text{max}}$ . If  $n < n_{\text{max}}$ , the decrease in  $R$  will cause  $n$  to fall further. Thus, the only the high- $n$  side of each peak is stable, and the dc value of  $n$  depends on the available power  $P_{\text{rf}}$ . The sharpness of this peak decreases with collisional damping, as shown in Fig. 12 under the standard conditions given above.

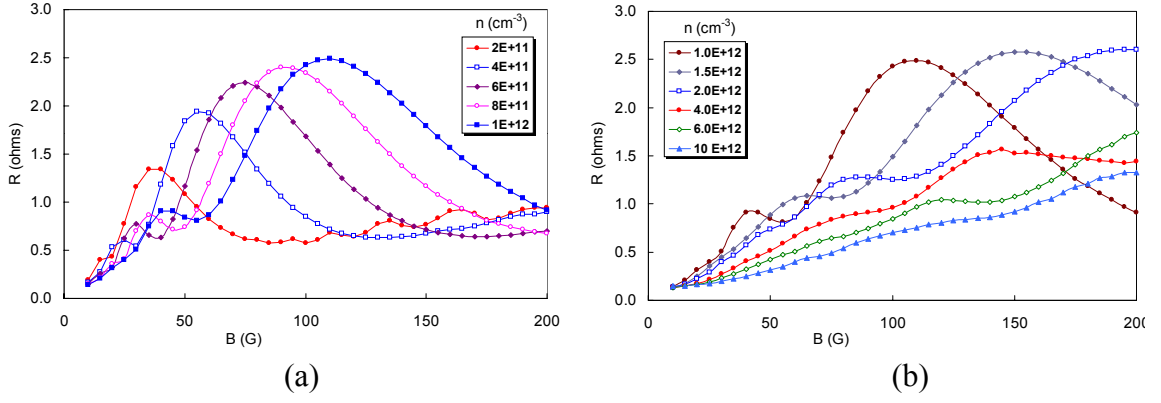


Fig. 9. Plasma loading resistance vs.  $B$  for (a) low and (b) high values of  $n$ .

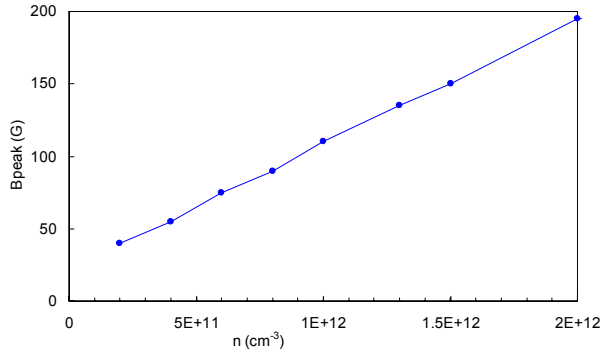


Fig. 10. Location of the low- $B$  peak vs. density

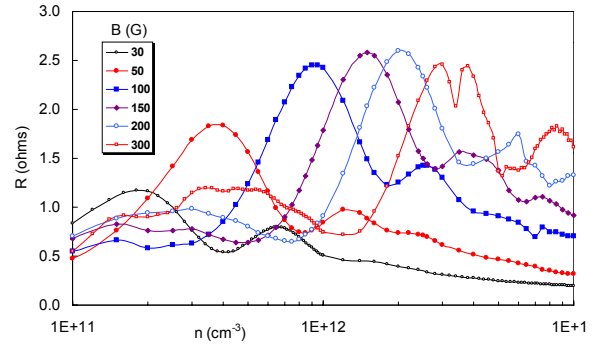


Fig. 11. The low- $B$  peak vs.  $n$  at constant  $B$ .

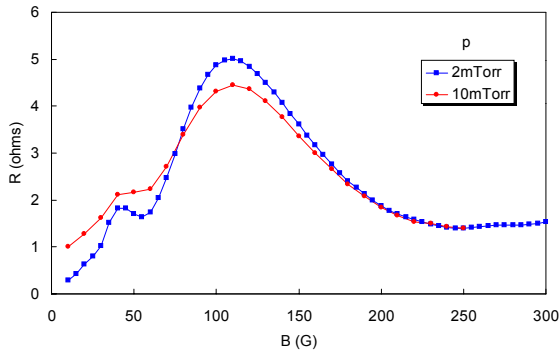


Fig. 12. The low- $B$  peak at 2 and 10 mTorr for  $n = 10^{12} \text{ cm}^{-3}$  and  $B = 100 \text{ G}$ .

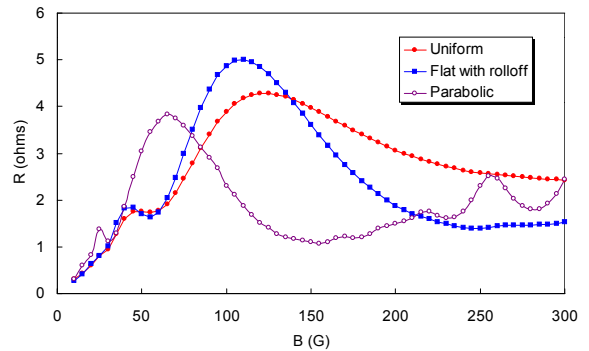


Fig. 13. The low- $B$  peak with different  $n(r)$  under standard conditions: (■)Standard profile, (◆) uniform plasma, and (○) parabolic profile.

The cause of the low- $B$  peak is certainly not the lower-hybrid resonance, which occurs at 1450 G for 13.56 MHz. It could be due to a resonance between the helicon and T-G waves, which could have similar radial wavelengths at low  $B$ . It could also be due to constructive interference between the forward wave and the wave reflected from the endplate. To distinguish between these two possibilities, several test runs were made. Figure 13 shows the effect of changing the density profile. Both the position and the magnitude of the peak are sensitive to  $n(r)$ , suggesting that the TG resonance may be responsible. However, Fig. 14 shows that changing the endplate from insulating to conducting greatly changes the nature of the low- $B$  peak, suggesting that reflection from the end is responsible. Figure 15 provides a

definitive test: As the loop antenna is moved from 10 cm to 5 cm in front of the endplate, the low- $B$  peak is changed; and if the plate is removed altogether, the peak no longer exists. There are a number of small peaks which appear in that case, and these could be due to the TG effect.

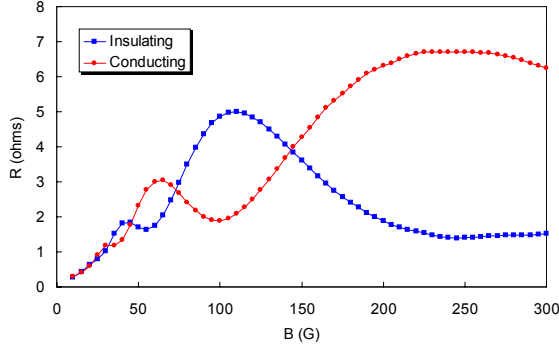


Fig. 14. Effect of the endplate material on the low- $B$  peak.

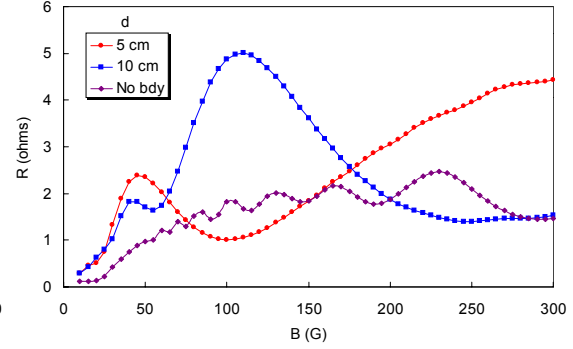


Fig. 15. Effect of antenna position on the low- $B$  peak.

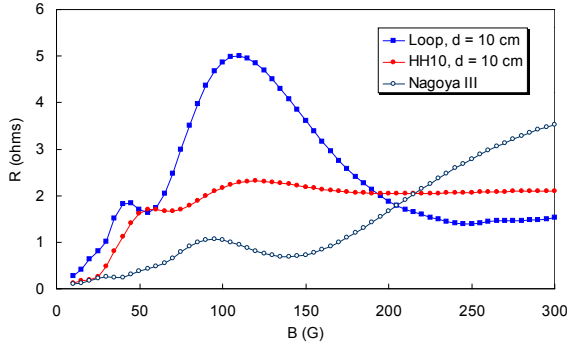


Fig. 16. Comparison of an  $m = 0$  loop antenna (■) with  $m = 1$  helical (◆) and Nagoya Type III (○) antennas.

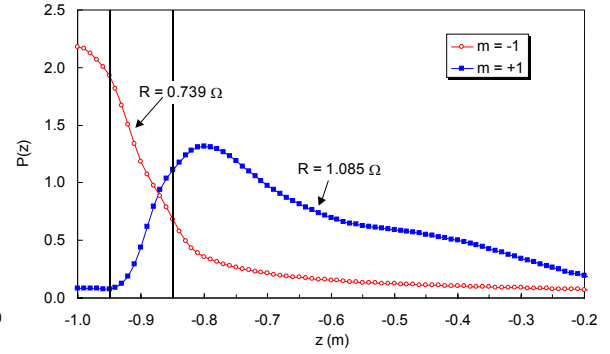


Fig. 17. Axial distribution of absorbed power for the 10-cm half-helical antenna launching the  $m = +1$  mode to the right (■) and to the left (○). The antenna lies between the vertical lines.  $R$  is the plasma resistance in each case.

In Fig. 16 we compare the performance of an  $m = 0$  loop antenna with those of a half-wavelength helical (HH10)  $m = +1$  antenna and a Nagoya Type III (N3)  $m = \pm 1$  antenna in the low field region. The HH10 antenna is 10 cm long and centered at  $d = 10$  cm from the endplate. The low- $B$  peak is barely noticeable with it. This can be understood because this antenna launches only a very weak  $m = -1$  mode towards the endplate, so that the reflected wave is very small. The N3 antenna, on the other hand, is bidirectional, launching strong  $m = +1$  waves in both directions; hence the low- $B$  peak is more noticeable. The directionality of the HH10 antenna is clearly seen in Fig. 17, which shows how the energy deposition is distributed along  $\mathbf{B}$ . When  $\mathbf{B}$  is reversed so that the  $m = +1$  mode is directed to the left, the peak absorption is at the endplate, and the total loading is not as large as when that mode is directed downstream. Changing the lengths and positions of the  $m = 1$  antennas does not improve their low- $B$  performance. It appears that the  $m = 0$  loop antenna produces the largest low- $B$  peak.

#### IV. Application to other density enhancement techniques

At high values of  $n$  and  $B$ , the plasma resistance is so high that essentially all the applied power is delivered to the plasma, and there is no local maximum of  $n(B)$ . Nonetheless, reflection from endplates can explain previously obtained results on density enhancement by aperture limiters and cusped magnetic fields. In 1992, it was found<sup>9</sup> that the plasma density at given pressure and rf power could be doubled by adding an aperture limiter or endplate behind the antenna, or by shaping the magnetic field so that it diverged sharply behind the antenna. These techniques are illustrated in Fig. 18. Tests were made with endplates that were either conducting (carbon) or insulating (BN), with or without a 1-cm diam hole in the center. These plates could be placed downstream of the antenna or within it, where they acted as aperture limiters, or upstream of it, where they acted as endplates. The optimum position was near the upstream end of the antenna (the short end of the vacuum chamber), but the exact position was not critical as long as it was behind the antenna. Density enhancement could also be achieved by reversing the current in the two end coils (Fig. 18) so that the field lines diverged sharply into the chamber wall (as shown), effectively making it into an insulating endplate. A slight further improvement could be made by applying both techniques together.

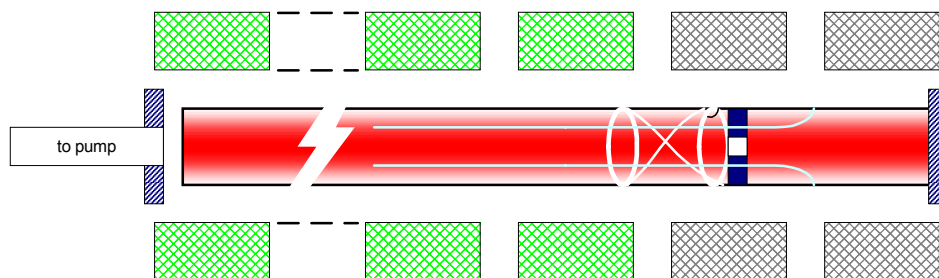


Fig. 18. Schematic of limiter and cusp experiments.

The effect of an endplate is illustrated in Fig. 19 for a density above  $10^{13} \text{ cm}^{-3}$  at  $800\text{G}^{10}$ , and the effect of a cusped field is shown in Fig. 20<sup>9</sup>. Both techniques are seen to increase  $n$  significantly at the same power. In Fig. 20, curves are shown for different field curvatures with the end coils turned off or reversed. In either case, the density integrated over the tube cross section is approximately a factor of two.

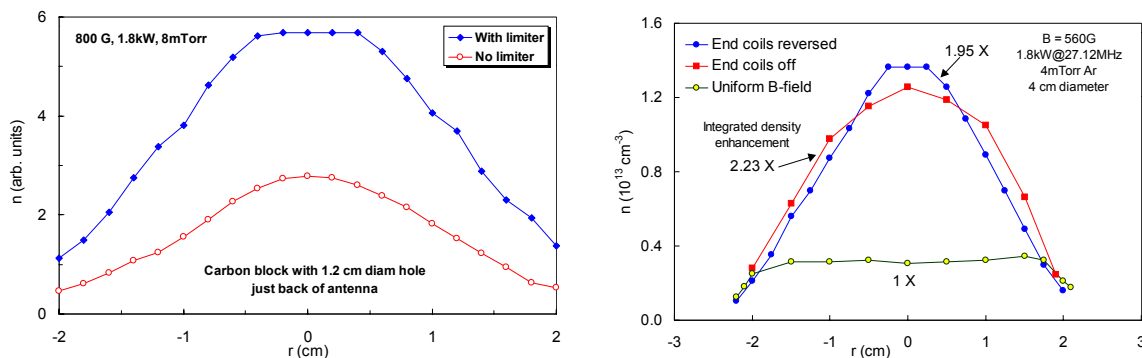


Fig. 19. Radial density profiles with and without an aperture limiter (Ref. 10).

Fig. 20. Radial density profiles in uniform and cusped magnetic fields (Ref. 9).

When the plasma resistance is computed for the conditions of these experiments, one finds that adding an endplate actually reduces the loading if  $n(r)$  is taken to have the standard shape shown in Fig. 5. It is essential to use the actual, measured  $n(r)$  profiles, which cannot be predicted without an equilibrium code. To see how an endplate affects energy deposition at high fields, we made a HELIC calculation for the parameters of Fig. 19. The result for  $P(z)$  in Fig. 21 shows that the presence of the endplate causes peaks in the collisional absorption and extends the range over which it occurs. The plasma resistance  $R$  increases from 1.21 to 1.97 $\Omega$ .

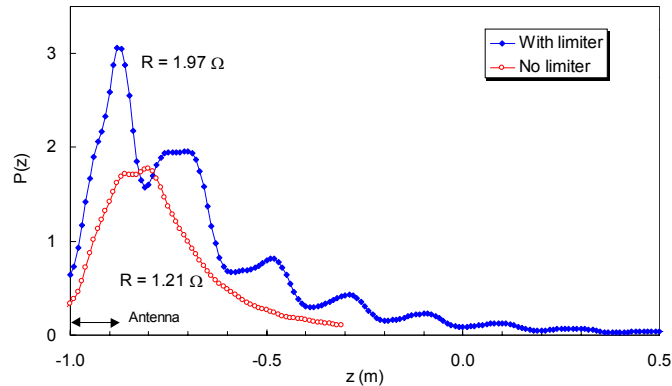


Fig. 21. Energy deposition  $P(z)$  along the B-field for the conditions of Fig. 19, with and without the aperture limiter. The antenna position is shown at the bottom left.  $R$  is the plasma resistance in each case.

## V. Conclusions

Reflection of helicon waves from surfaces behind the antenna can explain two previously unexplained experimental results: the occurrence of a low-field density peak and the factor-of-two density enhancement by endplates and magnetic cusps. These effects can be predicted by cold-plasma fluid codes which include the TG mode and the radial density profile. The low-B peak, in particular, is of interest for design of efficient reactors used in plasma processing.

## REFERENCES

\* Electronic address: ffchen@ee.ucla.edu

- <sup>1</sup> John D. Evans, private communication, 2001.
- <sup>2</sup> D. Arnush, Phys. Plasmas **7**, 3042 (2000).
- <sup>3</sup> S. Cho and J.G. Kwak, Phys. Plasmas **4**, 4167 (1997).
- <sup>4</sup> I.V. Kamenski and G.G. Borg, Computer Phys. Commun. **113**, 10 (1998).
- <sup>5</sup> Y. Mouzouris and J.E. Scharer, Phys. Plasmas **5**, 4253 (1998).
- <sup>6</sup> Th. Enk and M. Kraemer, Phys. Plasmas **7**, 4308 (2000).
- <sup>7</sup> B.H. Park, N.S. Yoon, and D.I. Choi, IEEE Trans. Plasma Sci. **29**, 502 (2001).
- <sup>8</sup> K.P. Shamrai and S. Shinohara, Phys. Plasmas **8**, 4659 (2001).
- <sup>9</sup> G. Chevalier and F.F. Chen, J. Vac. Sci. Technol. A **11**, 1165 (1993);
- <sup>10</sup> I. Sudit, unpublished, 1995.